ChemPubSoc Europe

DOI: 10.1002/chem.201704851

CHEMISTRY A European Journal Full Paper

C–H Bond Activation | *Very Important Paper*

VIP Acid-Triggered O–O Bond Heterolysis of a Nonheme Fe^{III}(OOH) Species for the Stereospecific Hydroxylation of Strong C–H Bonds

Joan Serrano-Plana,[a] Ferran Acuña-Parés,[a, b] Valeria Dantignana,[a] Williamson N. Oloo,[c] Esther Castillo,[d] Apparao Draksharapu,[c] Christopher J. Whiteoak,[a] Vlad Martin-Diaconescu,[a] Manuel G. Basallote,*[d] Josep M. Luis,*[a] Lawrence Que, Jr.,*[c] Miquel Costas,*[a] and Anna Company*[a]

Abstract: A novel hydroperoxoiron(III) species $[Fe^{III}(OOH)(MeCN)(PyNMe_3)]^{2+}$ (**3**) has been generated by reaction of its ferrous precursor $[Fe^{II}(CF_3SO_3)_2(PyNMe_3)]$ (**1**) with hydrogen peroxide at low temperatures. This species has been characterized by several spectroscopic techniques and cryospray mass spectrometry. Similar to most of the previously described low-spin hydroperoxoiron(III) compounds, **3** behaves as a sluggish oxidant and it is not kinetically competent for breaking weak C–H bonds. However, triflic acid addition to **3** causes its transformation into a much more reactive compound towards organic substrates that is capable of oxidizing unactivated C–H bonds with high stereospecificity. Stopped-flow kinetic analyses and theoretical studies provide a rationale for the observed chemistry, a triflic-acid-assisted heterolytic cleavage of the O–O bond to form a putative strongly oxidizing oxoiron(V) species. This mechanism is reminiscent to that observed in heme systems, where protonation of the hydroperoxo intermediate leads to the formation of the high-valent [(Porph$^{\bullet}$)Fe^{IV}(O)] (Compound I).

Introduction

Peroxoiron species are formed along the catalytic cycle of different nonheme iron proteins involved in important oxidative processes. Indeed, (hydro)peroxoiron compounds have been directly detected in natural systems such as Bleomycin,[1,2] a glycopeptide-based antitumor agent that carries out single- and double-stranded DNA cleavage,[3] and in Rieske oxygenases, a family of bacterial enzymes that catalyze the selective C–H hydroxylation of alkylarenes, and the stereo- and enantioselective *cis*-dihydroxylation of arenes.[4–6] Interestingly, the structure of a peroxo or hydroperoxo Fe^{III}(OO(H)) transient species has been solved by X-ray crystallography for two enzymes of the Rieske dioxygenase family, namely 1,2-naphthalene dioxygenase and carbazole 1,9a-dioxygenase.[7,8] Even though the Fe^{III}(OO(H)) moiety is the last detected species before substrate oxidation occurs, an intense debate exists on whether this species is directly responsible for the reactivity[9,10] or merely a precursor to a more reactive high-valent oxoiron species generated after homolytic or heterolytic O–O bond cleavage, for example, Fe^{IV}(O)/HO$^{\bullet}$or Fe^{V}(O)/HO^- respectively.[11,12]

In order to shed light into the structure and reactivity properties of these important iron-oxygen compounds, several nonheme hydroperoxoiron(III) species have been prepared using simple synthetic iron complexes bearing pyridine and amine-based ligands. Typically these species result from the reaction of an iron(II) precursor with excess hydrogen peroxide at low temperatures,[13,14] but in selected examples, they are generated by a combination of O_2 and a reducing agent.[15,16] From a chemical point of view, synthetic peroxoiron species are found to be rather unreactive towards organic substrates, a question that challenges the idea that they are the biological oxygenation agents.[12]

It is widely known that the cleavage of the O–O bond in Fe^{III}(OOH) species constitutes a key step in the O_2 activation mechanisms of natural heme enzymes such as cytochrome P450. In these systems, it is accepted that protonation of the distal oxygen atom of the Fe^{III}(OOH) compound (Cpd0) assists

[a] *Dr. J. Serrano-Plana, Dr. F. Acuña-Parés, V. Dantignana, Dr. C. J. Whiteoak, Dr. V. Martin-Diaconescu, Dr. J. M. Luis, Dr. M. Costas, Dr. A. Company Institut de Química Computacional i Catàlisi (IQCC) Departament de Química, Universitat de Girona C/ M. Aurèlia Capmany 69, 17003 Girona Catalonia (Spain) E-mail: joepm.luis@udg.edu miquel.costas@udg.edu anna.company@udg.edu*

[b] *Dr. F. Acuña-Parés Institute of Chemical Research of Catalonia (ICIQ) Avinguda Països Catalans 16, 43007 Tarragona (Spain)*

[c] *Dr. W. N. Oloo, Dr. A. Draksharapu, Prof. L. Que, Jr. Department of Chemistry and Center for Metals in Biocatalysis University of Minnesota, Minneapolis MN 55455 (USA) E-mail: larryque@umn.edu*

[d] *Dr. E. Castillo, Prof. M. G. Basallote Departamento de Ciencia de los Materiales e Ingeniería MetalúrgicayQuímica Inorgánica, Universidad de Cádiz, Facultad de Ciencias Apdo. 40, 11510 Puerto Real, Cádiz (Spain) E-mail: manuel.basallote@uca.es*

Supporting information and the ORCID identification number(s) for the author(s) of this article can be found under https://doi.org/10.1002/chem.201704851.

the heterolysis of the O–O bond, resulting in the formation of a high valent ferryl active species (CpdI) together with a water molecule.[17–19] Protonation of the OOH moiety has also been attempted in heme model systems. In line with the observations made in natural systems, the CpdI analogues in model systems are better formed under acidic conditions which trigger the O-O lysis of a Fe^{III}(OOH) precursor.[20,21]

Formation of Fe^{III}(OOH) and subsequent heterolytic O–O cleavage to form a highly electrophilic oxoiron(V) species have also been proposed to occur in the catalytic cycles of non-heme iron catalysts involved in alkane hydroxylation and alkene epoxidation using H_2O_2 as oxidant in the presence of carboxylic acids.[22–29] Direct evidence for this process was gained by Que and co-workers, who reported the water-assisted heterolytic O–O cleavage in $[Fe^{III}(OOH)(solvent)(tpa)]^{2+}$ (tpa = tris(2-pyridylmethyl)amine, solvent = H_2O or MeCN) leading to the formation of a high valent $Fe^{V}(O)$ species.[30] Moreover, acid-assisted homolytic or heterolytic O–O bond cleavage has been observed in non-porphyrinic iron model systems.[31–34] According to theoretical studies, O–O cleavage is also affected by the spin state on the iron(III) center. DFT calculations performed by Solomon and co-workers suggested that O–O bond homolysis in $S = 5/2$ systems is ≈ 10 kcal mol^{-1} higher in energy than in the low-spin counterparts ($S = 1/2$).[34,35] Finally, Que and co-workers reported that protonation of a high spin Fe^{III}(OOH) with $HClO_4$ led to the formation of an oxoiron(IV).[36] Recently, Nam, Sun and co-workers observed a dramatic enhancement of the reactivity of a mononuclear non-porphyrinic manganese complex towards alkenes upon addition of sulfuric acid when H_2O_2 was used as oxidant.[37] Mechanistic and reactivity studies pointed towards the involvement of a high valent Mn-oxo intermediate. Thus, acid-triggered O-O lysis arises as an interesting strategy to convert the relatively sluggish Fe^{III}(OOH) moieties into highly reactive oxoiron oxidants.

Recently, we reported that the reaction of $[Fe^{II}(CF_3SO_3)_2(PyNMe_3)]$ (**1**) with excess peracetic acid in acetonitrile at −40 °C generated a metastable brown species **2** that exhibited visible absorption features at $\lambda_{max} = 490$ and 660 nm with a 7:1 relative absorbance ratio (Scheme 1).[38] **2** proved to be highly active for the oxidation of alkanes with strong C–H bonds and alkenes, leading to the fastest oxidation rate described so far for synthetic iron–oxygen systems ($k_{cyclohexane} = 2.8$ M^{-1} s^{-1} at −40 °C, $k_{cyclooctene} = 375$ M^{-1} s^{-1} at −60 °C).[38,39] On the basis of a thorough EPR spectroscopic analysis, **2** was assigned as a mixture of two components in fast equilibrium: a major component corresponding to $[Fe^{V}(O)(OAc)(PyNMe_3)]^{2+}$ (40%) and a minor species regarded as $[Fe^{III}(OOAc)(PyNMe_3)]^{2+}$ (5%). Both EPR active species followed the kinetic trace of the 490 nm chromophore in the presence and absence of alkane or alkene substrate, thus indicating their direct relationship with the active species responsible for the oxidation event. In this work, we explore the reactivity of **1** with H_2O_2 (Scheme 1) and identify a hydroperoxoiron(III) species $[Fe^{III}(OOH)(MeCN)(PyNMe_3)]^{2+}$ (**3**) that exhibits enhanced reactivity towards alkanes in the presence of protons, which is directly related to the acid-triggered O–O cleavage observed in nature.[17–19]

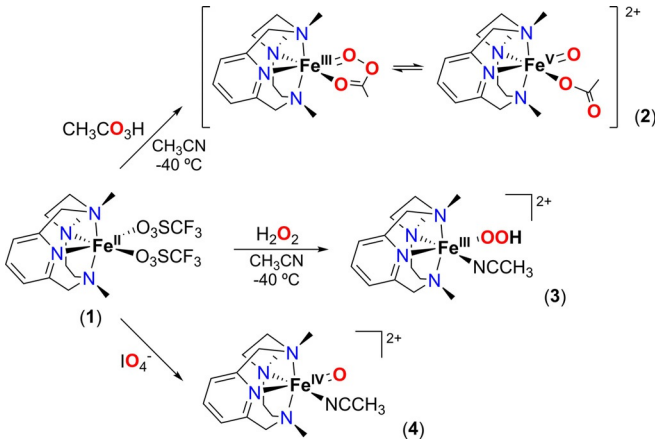

Scheme 1. Reactivity of **1** towards different oxidants to form the iron-oxygen species **2**, **3** and **4**.

Results and Discussion

Treatment of **1** with 10 equiv H_2O_2 in acetonitrile at −40 °C resulted in a clear color change from pale yellow to deep purple. UV/Vis absorption spectral monitoring of this process showed the formation of a band at 514 nm ($\varepsilon = 1600$ M^{-1} cm^{-1}, determined on the basis of the double integration of the EPR signal, see below) within 250 seconds (Figure 1a). This purple species (**3**) was not stable and disappeared over several minutes at −40 °C. Such a chromophore is reminiscent to those of previously reported low-spin Fe^{III}(OOH) species with tetra and pentadentate aminopyridine ligands, which exhibit an intense purple colour due to an absorption band at ~550 nm arising from peroxide-to-Fe^{III} charge transfer.[13,40,41] This formulation fully agreed with high-resolution cryospray mass spectrometric (CSI-MS) analyses conducted at −40 °C. The MS spectrum of **3** was dominated by a peak at $m/z = 486.0868$ with an isotopic pattern fully consistent with $[[Fe^{III}(OOH)(PyNMe_3)](CF_3SO_3)]^{+}$ (Figure 1b).

The resonance Raman spectrum of **3** in acetonitrile solution at −40 °C acquired with 561-nm excitation exhibits two resonantly enhanced bands at 614 cm^{-1} and 795 cm^{-1} (Figure 2a), which can be readily assigned to Fe–O and O–O stretching vibrations, respectively, due to their close resemblance to the resonance Raman features of other well-characterized low-spin Fe^{III}(OOH) species such as $[Fe^{III}(OOH)(TPA)]^{2+}$ (626 and 789 cm^{-1}, respectively) and $[Fe^{III}(OOH)(N4Py)]^{2+}$ (632 and 790 cm^{-1}, respectively).[42,43]

The EPR spectrum of **3**, obtained on a sample frozen at the maximum accumulation of its visible chromophore, clearly shows a low-spin $S = 1/2$ species with g-values 2.19, 2.16, 1.96 that accounts for ~53% of the iron content (Figure 2b and Supporting Information Figure S2). This signal could be easily fitted to the Taylor–Griffith model,[44,45] and is quite similar to those found for other low-spin Fe^{III}(OOH) species,[14] such as the well characterized $[Fe^{III}(OOH)(TPA)(solvent)]^{2+}$ ($g = 2.19$, 2.15, 1.97, solvent = MeCN or H_2O) and $[Fe^{III}(OOH)(N4Py)]^{2+}$ ($g = 2.16$, 2.11, 1.98) complexes.[42,43] There are also signals at

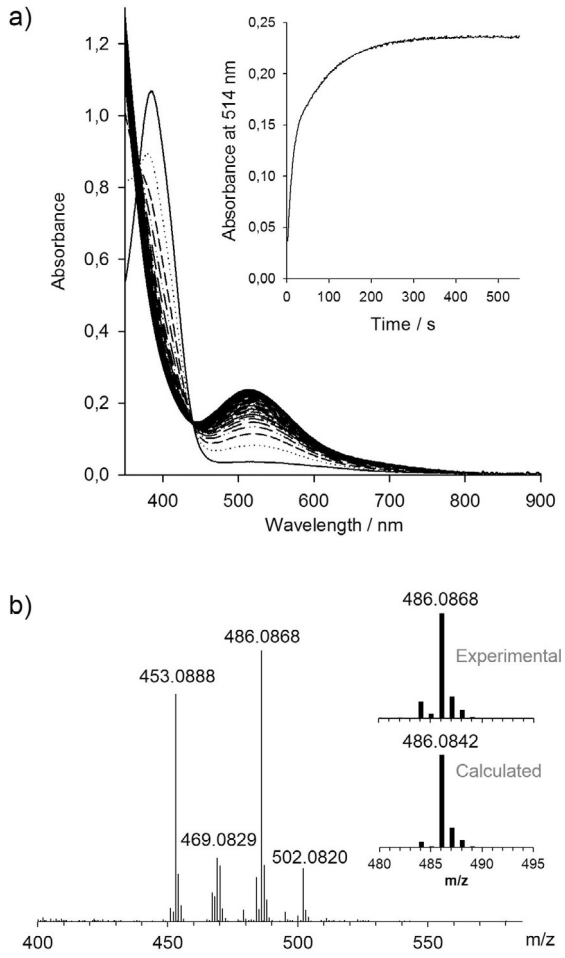

Figure 1. a) UV/Vis absorption spectral monitoring of the formation of **3** upon reaction of **1** (0.3 mM) with 10 equiv H_2O_2 in acetonitrile at −40 °C. Inset: kinetic trace at 514 nm. b) CSI-MS of **3** generated by adding H_2O_2 (10 equiv) to **1** in acetonitrile at −40 °C. The peak at *m/z* 453.0888 corresponds to the starting iron(II) complex $[[Fe^{II}(PyNMe_3)](CF_3SO_3)]^+$. Inset: calculated spectra for $[[Fe^{III}(OOH)(PyNMe_3)](CF_3SO_3)]^+$ with *m/z* = 486.0842 and comparison with the experimental pattern.

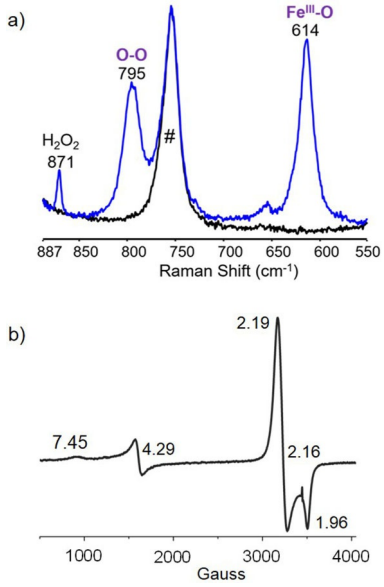

Figure 2. a) Resonance Raman spectrum of **3** (1.2 mM, blue) and its decayed species (black) in MeCN. # indicates a solvent-derived feature. 871 cm^{-1} band originated from excess H_2O_2 present in the solution. Spectra were acquired at −40 °C with 561-nm excitation. b) X-band EPR spectrum of **3** in frozen MeCN (T = 20 K, power = 0.2 mW, modulation amplitude = 1 mT).

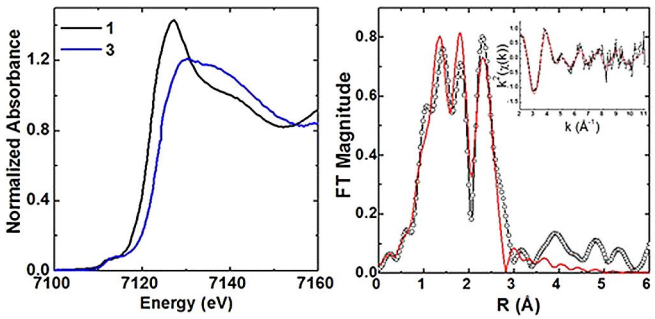

Figure 3. Fe K-edge XAS spectra: (left) XANES spectra of **1** and **3**; (right) Fourier transformed EXAFS spectra of **3** (inset: k^2-weighted unfiltered EXAFS spectra). Data: black circles; Fits: red line.

g = 7.45 and 4.29, which likely arise from high-spin (S = 5/2) ferric byproducts (Figure 2b).

This assignment is further supported by XAS (X-ray absorption spectroscopy) data (Figure 3). Compound **3** exhibits a rising edge energy at 7123.4 eV, ≈2 eV higher than that found for the starting iron(II) compound **1**, consistent with an iron(III) center.[46–49] Furthermore, EXAFS analysis of **3** shows a six-coordinate metal center with 0.6 N/O atom at 1.82 Å (to match the percentage of **3** present in the sample), 2 N/O atoms at 1.97 Å and 3 N/O atoms at 2.17 Å (see Supporting Information, Table S1), compared to **1**, which has a first coordination sphere having 2 N/O atoms at 2.05 Å and 4 N/O atoms at 2.19 Å (Figure S1, Table S1). In particular, the 1.82-Å scatterer found for **3** can be assigned to the O-atom of an HOO ligand, as observed at 1.76 and 1.81 Å in the EXAFS analysis of two related low-spin Fe^{III}(OOH) complexes.[43,46]

A detailed kinetic study on the formation and disappearance of **3** in acetonitrile solution was carried out using a cryo-stopped-flow instrument with a diode-array detector. When **1** reacts with an excess of H_2O_2 a biphasic kinetic behavior is observed. Under these conditions, the starting complex is converted to **3**, which disappears in a slower step. Formation of **3** occurs through a Fenton-like process involving the generation of an hydroxoiron(III) species or by mediation of an oxoiron(IV) compound that would comproportionate with unreacted **1** to give the iron(III) species, but such processes are indistinguishable with the current kinetic data. The rate constants for the first step (**1** → **3**) show a linear dependence on the concentration of H_2O_2 (Figure S5, left) with a second-order rate constant $k_{1\rightarrow3} = (4.8 \pm 0.8)\ M^{-1}\,s^{-1}$ at −35 °C. Species **3** disappears in a second, much slower step with a rate constant $k_{3\rightarrow C} = (1.2 \pm 0.1) \times 10^{-4}\ s^{-1}$ at −35 °C, which is independent of the concentration of oxidant.

Despite the fact that many hydroperoxoiron(III) species have been reported over the last decades, most of them bear tetradentate equatorially coordinated or pentadentate ligand archi-

tectures.[13] In contrast, **3** is one of the few examples having a tetradentate ligand that wraps around the metal center to make two labile *cis* positions available for interaction with the oxidant.[40,42,50–53] Given the relative stability of **3**, reactivity studies could be performed for this species (see below).

Reaction of **1** with oxygen-atom donors such as periodate were also studied. Thus, UV/Vis monitoring of a solution containing **1** and Bu_4NIO_4 (1.1 equiv) in MeCN at −40 °C showed the immediate quenching of the absorption features associated with the starting iron(II) complex (**1**) and the appearance of two weak bands at 802 and 983 nm, commonly associated with d–d transitions of $S=1$ oxoiron(IV) species (Figure S3).[54] Further confirmation of this formulation was achieved by CSI-MS analysis conducted at −40 °C, which showed a major peak at $m/z=469.0820$ with an isotopic distribution pattern fully consistent with $[Fe^{IV}(O)(CF_3SO_3)(PyNMe_3)]^+$ (Figure S4).

Reaction of 3 with H^+ and its influence on HAT reactions

Nonheme $Fe^{III}(OOH)$ intermediates are currently regarded as rather sluggish oxidants.[55] Indeed, addition of different substrates susceptible to undergo oxidation after maximum formation of **3** at −25 °C did not cause any apparent change in the decay rate of its characteristic absorption band. This was observed both for substrates susceptible to be attacked by a nucleophilic oxidant (2,2,2-trifluoroacetophenone) and for those susceptible to be attacked by an electrophilic oxidant (alkanes, alkenes, R_2S or phosphines). However, analysis of the reaction mixture after the complete self-decay of the chromophore revealed the formation of oxidized products. The fact that the addition of these substrates to **3** does not affect its decomposition, indicates that this species is not kinetically competent to perform their oxidation. This, therefore, must be executed by iron-based or organic radical oxidizing species formed upon the decomposition of **3**. Analysis of the organic products indicated that the oxidation process was poorly selective. For example, oxidation of cyclohexane afforded a mixture of cyclohexanol (A) and cyclohexanone (K) with an A/K ratio of 0.6 and a combined 95% yield (with respect to Fe content, Figure 4). This A/K ratio suggests the involvement of long-lived carbon-centered radicals that are readily trapped by O_2.

Interestingly, addition of triflic acid (TfOH, 1.1 equiv with respect to iron) at maximum formation of **3** at −25 °C caused the immediate decay of its visible absorption band at 514 nm. Most surprisingly, and in sharp contrast to the acid-free system, analysis of the reaction mixture after the addition of triflic acid to a solution of **3** containing cyclohexane (50 equiv) showed the formation of cyclohexanol (A) and cyclohexanone (K) with a A/K ratio of 4.0 in a combined 80% yield (with respect to Fe, Figure 4). Substitution of cyclohexane by *cis*-1,2-dimethylcyclohexane afforded the corresponding tertiary alcohol product in 39% yield with relatively high stereoretention (80%). In contrast, the absence of acid gave much lower yields of tertiary alcohols (7%),[56] with predominant inversion of configuration (retention of configuration (RC) = −38%). Similar results were obtained with *cis*-decaline for which yields of tertiary alcohols increased from 14 to 38% and stereoretention

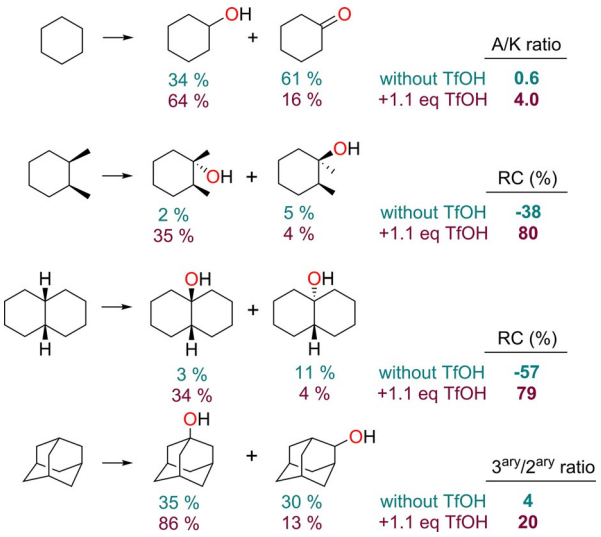

Figure 4. Oxidation of different alkanes by **3** in the presence or absence of triflic acid (TfOH). Yields (%) with respect to iron content are shown below each compound and were determined by GC.

changed from 79% to −57% when TfOH was added to the reaction of **3** with this substrate. Finally, the addition of adamantane (10 equiv) to **3** afforded a high selectivity for the tertiary C–H site in the presence of acid (normalized $3^{ary}/2^{ary}$ ratio = 20), while this value decreased to 4 in the acid-free system (Figure 4). Importantly, no oxidation products were obtained in the corresponding blank experiments in the absence of iron complex.

The clear-cut differences in regio- and stereospecificities highlight the involvement of oxidants of different nature in the oxidation reactions carried out by **3** in the absence or presence of acid. Most probably, unselective hydroxyl radicals (HO·) and the oxoiron(IV) species (**4**) resulting from the homolytic cleavage of the O–O bond in **3** or related species together with long-lived carbon-centered radicals are responsible for the observed chemistry in the absence of acid. Instead, in the presence of acid formation of a highly selective metal-based oxidant is favoured, which may originate from the heterolytic O–O cleavage in **3**.

Some reports have disclosed that the interaction of oxoiron(IV) species with protons can promote their reactivity towards substrates.[57] In order to discard the involvement of such species in the observed reactivity of **3** in the presence of acid, a blank experiment was carried out. Thus, compound **4** (generated by reaction of **1** with IO_4^- as described above) was reacted at −25 °C with 50 equivalents 1,2-dimethylcyclohexane. Interestingly, the rate of decay of **4** was not significantly altered upon addition of the substrate. Eventually, after its decay, analysis of the reaction mixture afforded the corresponding tertiary alcohol products in a moderate 4% yield and with a low retention of configuration (27%). A similar result was obtained when 1.1 equiv of TfOH were added together with the substrate. The outcome of these experiments indicates that compound **4**, which might be formed by homolytic O–O cleavage of **3**, is not involved in the reaction of **3** + TfOH with C–H bonds, or alternatively it is only a minor component.

Kinetic analysis of the reaction of 3 with H^+

As the reaction between **3** and TfOH was very fast, it was further explored by means of sequential cryo-stopped-flow experiments at −35 °C. Experiments were carried out by adding 0.25–9 equivalents TfOH with respect to the starting iron complex once the characteristic band of **3** (formed by reaction of **1** with H_2O_2) at 514 nm reached its maximum intensity. Those experiments showed the rapid disappearance of the band typical of **3** without the appearance of any new band in the visible region of the spectra. Unfortunately the kinetics showed little reproducibility, probably because of the instability of acetonitrile solutions of TfOH.[58]

For this reason, the kinetic experiments were carried out using $[H(OEt_2)_2][BF_4]$ instead of TfOH. According to the pK_a values reported for $[H(OEt_2)_2][BF_4]$ and TfOH in acetonitrile (0.2 and 2.6, respectively),[59,60] both acids are expected to be essentially dissociated in acetonitrile solutions at the concentrations used in the kinetic studies, and so the reacting species is the solvated proton in both cases. In this line, similar results were obtained in the reactivity of **3** toward alkanes in the presence of any of the two acids. The spectral changes observed for the reaction between **3** and $[H(OEt_2)_2][BF_4]$ (0.7–10.0 equivalents in acetonitrile) were better behaved than those for TfOH, and they clearly revealed biphasic kinetics (**3**→I→P, Figure S6). The first step led to the disappearance of the band of **3** centered at 514 nm with a rate constant independent of the acid concentration and a value of $k_{3\rightarrow I}=(2.0\pm0.1)\times10^{-2}\ s^{-1}$ at −35 °C. The independence of the rate with the proton concentration can be interpreted by considering that the disappearance of **3** in the presence of acid occurs according to the mechanism indicated in Eqs. 1–2, that implies an initial rapid pre-equilibrium of formation of an adduct between **3** and the proton. The rate law for this mechanism (Eq. 3) simplifies to $k=k_{O-O}$ if the equilibrium in Eq. 1 is considered to be displaced to the right hand side.

$$\mathbf{3} + H^+ \rightleftharpoons \mathbf{3}\cdot H^+ \qquad K_H \tag{1}$$

$$\mathbf{3}\cdot H^+ \rightarrow I \qquad k_{O-O} \tag{2}$$

$$k_{3\rightarrow I} = \frac{k_{o-o}K_H[H^+]}{1+K_H[H^+]} \tag{3}$$

Following the disappearance of the hydroperoxo species, there were additional slower spectral changes in the UV region that occurred with a rate constant that is also independent of acid concentration, $k_{I\rightarrow P}=(7\pm2)\times10^{-4}\ s^{-1}$. Importantly, the rate of decay of I is also independent of the presence of alkane substrates, thus suggesting that the intermediate I detected in the stopped-flow experiments is not responsible for substrate oxidation, but it probably results from the rapid transformation of a more reactive species that is not detected under our experimental conditions.

Overall, the decay of **3** is triggered by acid to generate a highly reactive species that hydroxylates C–H bonds in a stereospecific manner, as experimentally observed (see experiments above). However, this species is unfortunately not detectable, even under stopped-flow conditions, and evolves into unreactive species I.

DFT calculations for the reaction of 3 with H^+

Especially intriguing was the nature of the highly selective metal-based oxidant involved in the reactions of **3** in the presence of 1 equiv of acid. We speculated about the possibility of a protonation step of the OOH moiety in **3**, which would lead to the loss of one water molecule to promote the heterolytic cleavage of the O–O bond. The resulting compound would be putatively a highly electrophilic oxoiron(V) species, which are known to be powerful and stereoretentive oxidizing agents (Scheme 2). Formation of such species would explain the selectivity patterns experimentally observed in the oxidation of alkanes.

In order to study the feasibility of accessing the oxoiron(V) after protonation of the ferric hydroperoxo moiety, DFT studies were performed (see computational details). The low spin nature of **3,** as ascertained by EPR, strongly suggests the presence of a sixth, strong field ligand. Acetonitrile is the most plausible candidate since **3** is generated in this solvent, so that the general formula of **3** corresponds to $[Fe^{III}(OOH)(MeCN)(PyNMe_3)]^{2+}$, where the OOH ligand coordinates in an end-on fashion. A hydroperoxoiron(III) species with a side-on bound hydroperoxide ligand was also considered in our calculations, but all our attempts to optimize this geometry ended up in the end-on compound, pointing out that the most stable conformer is given by the end-on coordination of OOH to the iron.

The hydroperoxide can be bound at any of the two available *cis* labile positions of complex **3**, which leads to two possible tautomeric structures: one with the OOH group *cis* to the pyri-

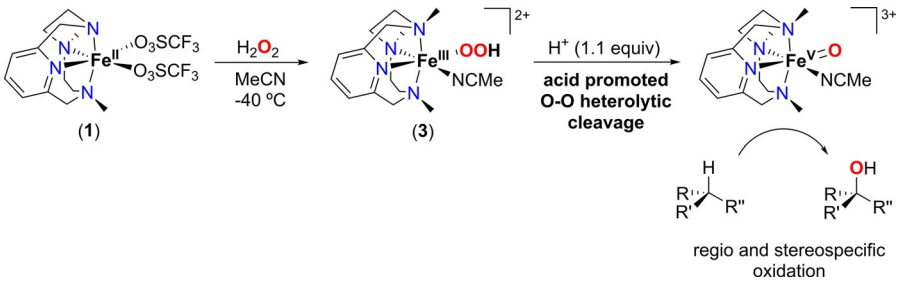

Scheme 2. Formation of compound **3** from **1** and its reactivity towards substrates.

dine ring ($Fe^{III}(OOH)_A$) and another with a relative *trans* disposition of these moieties ($Fe^{III}(OOH)_B$) (see Figure S7 for optimized structures). DFT calculations at −40 °C taking into account thermal and entropic corrections reveal that the two tautomers in the $S=1/2$ spin state are quasi isoergonic, with a free energy difference of only 0.6 kcal mol^{-1}, which is lower than the average error of our theoretical approach. Therefore, both isomers could exist in solution. It is worth mentioning here that theoretical calculations indicate that the $S=5/2$ spin state of $Fe^{III}(OOH)_A$ and $Fe^{III}(OOH)_B$ are 2.6 kcal mol^{-1} and 2.1 kcal mol^{-1} more stable than the $S=1/2$ isomers, respectively, in disagreement with the low-spin state experimentally determined for **3**. This might be rationalized by the fact that B3LYP tends to over stabilize the high-spin states. For this reason, the low spin $S=1/2$ was used for our calculations in order to reproduce experimental data.

The homolytic and heterolytic O–O bond cleavage mechanisms by **3** were explored in the absence and presence of acid at −40 °C, respectively, including the effect of the proton, acetonitrile and water concentrations. For convenience, the isomer $Fe^{III}(OOH)_A$ was chosen to perform the DFT mechanistic study. In the absence of TfOH, the homolytic O–O bond cleavage, which exclusively proceeds through the $S=1/2$ spin energy surface, is strongly endergonic ($\Delta G=19.7$ kcal mol^{-1}) and has a barrier of 20.7 kcal mol^{-1} (Figure 5). This is in agreement with the long half-life time of **3** at −40 °C. In the transition state ($TS_{A\_homo\_d}$) the O–O bond has been elongated by 1.01 Å with respect to the $Fe^{III}(OOH)_A$ compound (3_{A_d}) and an ·OH radical is already generated (Mulliken spin density located on OH, $\rho(O_bH)=-0.95$) (see Figure S8 for the most relevant geometrical data). The O–O bond cleavage and the formation of a hydrogen bond between the OH fragment and the oxo ligand proceed in a concerted manner until a highly energetic Fe=O···HO· adduct is obtained. The Mulliken spin density analysis and the Fe–O bond distance of this product are consistent with a $S=1$ $Fe^{IV}(O)$ moiety ($\rho(Fe)=1.41$, $\rho(O_a)=0.69$, d(Fe-O)= 1.646 Å) antiferromagnetically coupled to a HO· radical ($\rho(O_b)=-1.0$). Thus, DFT calculations support that $Fe^{IV}(O)$ (**4**) is slowly formed along the self-decay of **3**. Moreover, the simultaneous generation of a HO· is in agreement with the observed radical character of the alkane oxidation performed by **3** under acid-free conditions.

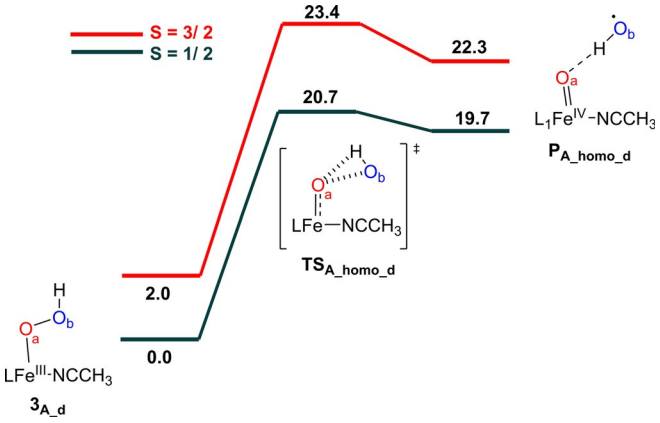

Figure 5. Free energy profile of the homolytic O–O bond cleavage of **3** at −40 °C in the $S=1/2$ and $S=3/2$ spin surfaces. The $PyNMe_3$ ligand is represented by label L.

Under our experimental conditions, however, the characteristic UV-vis absorption bands corresponding to **4** were not observed along the self-decay of **3** in the absence of acid. This can be explained by the rapid reaction of **4** with excess peroxide present in the reaction mixture (10 equiv H_2O_2 are necessary to maximize the formation of **3**). This hypothesis was experimentally supported by examining the reaction between **4**, generated by reaction of **1** with Bu_4NIO_4, and H_2O_2, which proceeded very rapidly at −25 °C (within mixing time of the reagents).

As suggested by experimental data, heterolytic O–O bond cleavage could be assisted by the protonation of the OOH moiety when TfOH is present in the reaction media. To corroborate this hypothesis, three different mechanisms have been explored (Figures 6 and S10–S12 for complete energy profiles). Protonation of the oxygen atom directly connected to the iron center (O_a) and the subsequent intramolecular proton transfer to the distal oxygen of the OOH moiety (O_b) to generate a water molecule was kinetically unfeasible under the reaction conditions ($\Delta G^{\ddagger}=49.2$ kcal mol^{-1}; Figure S10).

The high concentration of acetonitrile molecules (19.1 M) suggests that the organic solvent could also assist the proton transfer to the OOH fragment.[61] Indeed, the inclusion of two explicit MeCN molecules is essential for the correct evaluation of the heterolytic bond cleavage barrier. The free energy profile for the heterolytic mechanism is presented in Figure 6. The reaction evolves in the $S=1/2$ spin surface until final formation of a $[Fe^{V}(O)(MeCN)(PyNMe_3)]^{3+}$ complex (optimized geometries are shown in Figure S9). The free energy penalty for the interaction of the proton with the O_bH moiety of the 3_{A_d} complex and its solvation with two acetonitrile molecules ($R_{A\_heter\_d}$) is 4.6 kcal mol^{-1}. In the transition state ($TS_{A\_heter\_d}$) the O–O bond cleavage and the proton transfer to O_b atom occur in a concerted manner ($\Delta G^{\ddagger}=14.9$ kcal mol^{-1}). Interestingly, the slight elongation of the O–O bond in $TS_{A\_heter\_d}$ (0.37 Å with respect to $R_{A\_heter\_d}$) and the proton displacement promote the spin density transfer from the Fe-O moiety to the incipient water molecule ($\rho(Fe-O)=1.44$, $\rho(H_2O)=-0.31$). Then the reaction evolves to the formation of a formal $Fe^{V}(O)$ compound ($\rho(Fe\text{-}O)=1.51$, d(Fe–O) = 1.638 Å) and a solvated water molecule which still has a significant beta spin density ($\rho(H_2O)=-0.36$). Finally, the release of the generated water molecule from the first solvation shell of $[Fe^{V}(O)(MeCN)(PyNMe_3)]^{2+}$ leads to the stabilization of the $S=3/2$ spin state. The kinetics of the latter mechanism were also modelled considering that the proton is shuttled to O_b by a hydronium cation (Figure S11). However, due to the low concentration of water in the reaction mixture (estimated to be 5 mM), the free energy of the barrier of the O–O heterolytic cleavage increases by 4.7 kcal mol^{-1} with respect to the DFT mechanism with a proton solvated by an acetonitrile shown in Figure 6.

In the literature it has been also reported that the intramolecular protonation of the hydroperoxide moiety assisted by an aqua ligand in *cis*-relative position may lead to the formation

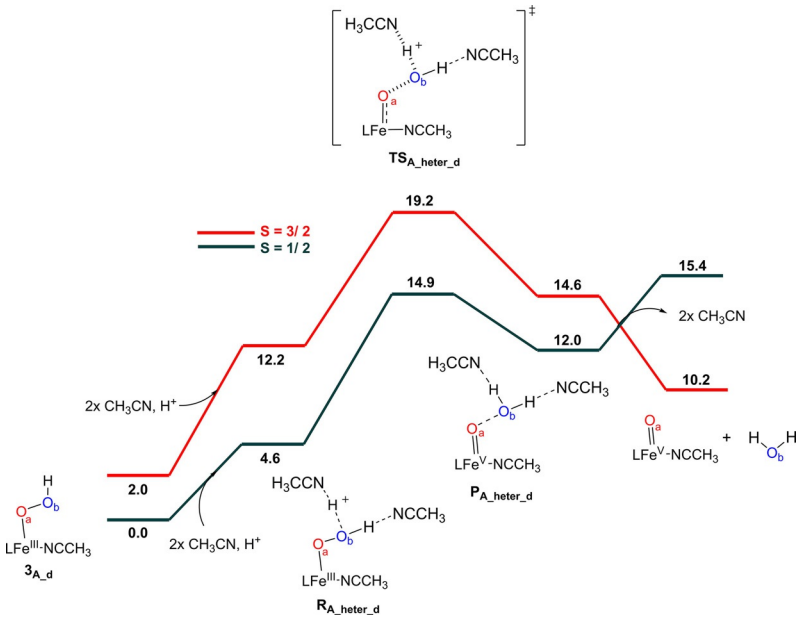

Figure 6. Free energy profile of the acid-triggered acetonitrile-assisted heterolytic O–O bond cleavage mechanism at −40 °C in compound **3** ($S=1/2$ and $S=3/2$ spin surfaces are shown). The $PyNMe_3$ ligand is represented by label L.

of $Fe^{V}(O)$ species.[28] The same mechanism was considered for $[Fe^{III}(OOH)(H_2O)(PyNMe_3)]^{2+}$, but a higher barrier was obtained ($\Delta G^{\neq}=21.2$ kcal mol^{-1}) with respect to the acetonitrile assisted mechanism (Figure S12). Moreover, this process would not account for the key effect of the acid on the generation of the $Fe^{V}(O)$ species. Therefore, DFT calculations suggest that the most plausible O–O bond cleavage mechanism under acidic conditions is a heterolytic O–O cleavage which leads to the formation of a $[Fe^{V}(O)(MeCN)(PyNMe_3)]^{2+}$ compound.

Comparison of theoretical with experimental data

In order to compare the results of the DFT studies with the experimental data, the activation parameters for the decomposition of **3** both in the absence and presence of acid were obtained. The values in the absence of acid were $\Delta H^{\neq}=(10.4\pm0.7)$ kcal mol^{-1} K^{-1} and $\Delta S^{\neq}=-(33\pm3)$ cal mol^{-1} K^{-1}, whereas in the presence of acid $\Delta H^{\neq}=(11\pm1)$ kcal mol^{-1} K^{-1} and $\Delta S^{\neq}=-(19\pm3)$ cal mol^{-1} K^{-1}. These values lead to $\Delta G^{\neq}$ values at −40 °C of 18.1 and 15.4 kcal mol^{-1} in the absence and in the presence of acid, respectively, in good agreement with the computational results. The activation enthalpy is in both cases close to values reported in the literature for decomposition of other $Fe^{III}(OOH)$ complexes.[12,62,63] However, whereas the negative $\Delta S^{\neq}$ observed in the presence of acid can be rationalized by considering acid attack before the rate determining step, the more negative value obtained in the absence of acid does not appear reasonable for an intramolecular process and it suggests the participation of another non-identified species such as H_2O, or excess H_2O_2, for example.

According to the mechanism in Figure 6, the disappearance of **3** in the presence of acid would agree with the mechanism indicated in Eqs 1–2, in line with the experimental observations. Importantly, the agreement between the DFT-calculated activation barrier ($\Delta G^{\neq}=14.9$ kcal mol^{-1} at −40 °C) and that derived from kinetic measurements ($\Delta G^{\neq}=15.4$ kcal mol^{-1} at −40 °C) is excellent, thus supporting the occurrence of heterolytic breaking of the O–O bond through this mechanism.

Conclusion

In summary, we have characterized a novel low-spin hydroperoxoiron(III) species (**3**) formed after the reaction of hydrogen peroxide and the ferrous precursor bearing the macrocyclic ligand $PyNMe_3$. Its reactivity, similarly to related systems, is sluggish. However, we have observed that the addition of acid rapidly causes the decomposition of such species by promoting the heterolytic O–O cleavage to form a putative $Fe^{V}(O)$ species that shows dramatic differences in reactivity. Indeed, protonation of an Fe–OOH moiety precedes the formation of the highly reactive $Fe^{IV}(O)$–porphyrin radical cation oxidant in heme systems. Thus, we suggest that for **3** a similar stepwise process occurs, which is supported by DFT calculations.

Experimental Section

Materials. Reagents and solvents used were of commercially available reagent quality unless otherwise stated. Solvents were purchased from Scharlab, Acros or Sigma–Aldrich and used without further purification. Preparation and handling of air-sensitive materials were carried out in a N_2 drybox (Jacomex) with O_2 and H_2O concentrations <1 ppm. $PyNMe_3$ and $[Fe^{II}(OTf)_2(PyNMe_3)]$ (**1**) were prepared following previously described procedures.[38,39]

Physical methods. High resolution mass spectra (HRMS) were recorded on a Bruker MicrOTOF-Q IITM instrument using ESI or Cryospray ionization sources at Serveis Tècnics of the University of Girona. Samples were introduced into the mass spectrometer ion source by direct infusion using a syringe pump and were externally calibrated using sodium formate. A cryospray attachment was

used for CSI-MS (cryospray mass spectrometry). Temperature of the nebulizing and drying gases was set at −40 °C. The instrument was operated in positive ion mode.

NMR experiments were performed on a Bruker Ultrashield Avance III400 and Ultrashield DPX300 spectrometers.

UV/Vis spectroscopy was performed with an Agilent 50 Scan (Varian) UV/Vis spectrophotometer with 1 cm quartz cells. Low temperature control was achieved with a cryostat from Unisoku Scientific Instruments, Japan.

GC product analyses were performed on an Agilent 7820A gas chromatograph equipped with a HP-5 capillary column 30mx0.32mmx0.25 μm and a flame ionization detector.

Stopped-flow experiments were carried out using an SFM4000 Bio-logic instrument provided with a cryo-stopped-flow accessory fitted to a Huber CC-905 bath.

Perpendicular (9.63 GHz) mode X-band EPR spectra were recorded on a Bruker EPP 300 spectrometer equipped with an oxford ESR 910 liquid helium cryostat and an Oxford temperature controller. The quantification of the signals was relative to a Cu-EDTA spin standard. Software for EPR analysis was provided by Dr Michael P. Hendrich of Carnegie Mellon University.

Resonance Raman spectra were obtained at −40 °C with excitation at 561 nm (100 mW at source, Cobolt Lasers) through the sample in a flat bottom NMR tube using a 90° scattering arrangement (parallel to the slit direction). The collimated Raman scattering was collected using two Plano convex lenses (f = 12 cm, placed at an appropriate distance) through appropriate long pass edge filters (Semrock) into an Acton AM-506 m3 monochromator equipped with a Princeton Instruments ACTON PyLON LN/CCD-1340×400 detector. The detector was cooled to −120 °C prior to the experiments. Spectral calibration was performed using the Raman spectrum of acetonitrile/toluene 50:50 (v:v).[64] Each spectrum was accumulated, typically 20 times with a 3-s acquisition time for a total acquisition time of 1 min per spectrum. The collected data was processed using Spekwin32, and a multi-point baseline correction was performed for all spectra.

Samples for X-ray absorption (XAS) were prepared as 2 mM solutions in acetonitrile and loaded into 2 mm Delrin holders having Kapton tape windows. Samples were stored at liquid nitrogen temperatures until run. XAS data was collected at the SOLEIL synchrotron SAMBA beamline equipped with a Si(220) double crystal monochromator, under anaerobic conditions using a liquid helium cryostat (20 K). The absorption signal was detected in fluorescence mode using a Canberra 35 element Ge detector and a Z-1 filter. The Athena software package and AUTOBK algorithm were used for data reduction. Furthermore, energy was calibrated using the first inflection point of the XAS spectrum of iron foil at 7111.2 eV. EXAFS were extracted using a R_{bkg} of 1 Å and a spline to a k of 13.4 $Å^{-1}$. EXAFS were analyzed using the Artemis software package employing the iFEFFIT engine and FEFF6 code.[65–67] The k^2-weighted data was fit in r-space over a k-rage of 2–11 $Å^{-1}$, with an S_0 value of 0.9 and a Hanning window (dk 1). The spectra were not phase corrected and a global ΔE_0 was employed, with the initial E_0 set to the inflection point of the rising edge. Single scatter paths for Fe-N as well as multiple scattering from the ligand backbone were fit in terms of ΔR_{eff} and σ^2 as previously described.[68–70] To assess the goodness of fit from different models both the R_{factor} (%R) and the reduced χ^2 (χ^2_ν, defined as equivalent to $\chi^2/(N_{idp}-N_{var})$ where N_{var} is the number of refining parameters) were minimized. While the R_{factor} is generally expected to decrease with the number of adjustable parameters, χ^2_ν may eventually increase, indicating the model is over-fitting the data.[71] Lastly fits were performed using the general EXAFS formula:

$$\chi(k) = S_0^2 \sum_i \frac{N_i S_i(k) F_i(k)}{kR_i^2} e^{-2R_i/\lambda(k)} e^{-2\sigma_i^2/k^2} \sin[2kR_i + \varphi_i(k)]$$

With χ^2 and R_{factor} are defined as:

$$\chi^2 = \frac{N_{idp}}{N_{pts}\varepsilon^2} \sum_{i=1}^{N} \{[Re(\chi_{data}(R_i) - \chi_{theory}(R_i))]^2 + [Im(\chi_{data}(R_i) - \chi_{theory}(R_i))]^2\}$$

In which N_{idp} is the number of independent data points defined as $N_{idp} = 2\Delta k \Delta r/\pi$; Δr is the fitting rang in *r*-space; Δk is the fitting range in *k*-space; N_{pts} is the number of points in the fitting range; ε is the measurement of uncertainty; *Re( )* is the real part of the EXAFS Fourier transformed data and theory functions; *Im( )* is the imaginary part of the EXAFS Fourier transformed data and theory functions; $\chi(R)$ is the Fourier transformed data or theory function; and

$$R_{factor} = \frac{\sum_{i=1}^{N} \{[Re(\chi_{data}(R_i) - \chi_{theory}(R_i))]^2 + [Im(\chi_{data}(R_i) - \chi_{theory}(R_i))]^2\}}{\{[Re(\chi_{data}(R_i))]^2 + [Im(\chi_{data}(R_i))]^2\}}$$

Generation of 3. In a typical experiment, a 1 mM solution of **1** in dry acetonitrile was prepared inside the glovebox. 2 mL of this solution were placed in a UV/Vis cuvette (2 μmols of **1**). The quartz cell was capped with a septum and taken out of the box, placed in the Unisoku cryostat of the UV/Vis spectrophotometer and cooled down to 238 K. After reaching thermal equilibrium an UV/Vis absorption spectrum of the starting complex was recorded. Then, 50 μL of a solution containing hydrogen peroxide (50% or 70% in water) in dry acetonitrile were added (20 μmols). The formation of a band at $\lambda_{max} = 514$ nm corresponding to **3** was observed. Full formation of **3** was achieved in ~ 200 s.

Reaction of 3 with organic substrates

For reactivity studies, **3** was generated following the same experimental procedure described above but setting the temperature to −25 °C.

Without added acid: once **3** was fully formed, 100 μL of a solution containing the corresponding equivalents of the desired substrate were added in the cuvette. Once the $\lambda_{max} = 514$ nm band was fully decayed, biphenyl was added as internal standard, and the iron complex was removed by passing the solution through a short path of silica. The products were then eluted with ethyl acetate and subjected to GC analysis.

With added acid: once **3** was fully formed, 100 μL of a solution containing the corresponding equivalents of the desired substrate were added in the cuvette, followed by the addition of 25 μL of a solution containing TfOH (1.1 equiv) in acetonitrile. The immediate bleaching of the chromophore was observed. Biphenyl was added as internal standard, and the iron complex was removed by passing the solution through a short path of silica. The products were then eluted with ethyl acetate and subjected to GC analysis.

Generation of 4. In a typical experiment, a 1 mM solution of **1** in dry acetonitrile was prepared inside the glovebox. 2 mL of this solution were placed in a UV/Vis cuvette (2 μmols of **1**). The quartz cell was capped with a septum and taken out of the box, placed in the Unisoku cryostat of the UV/Vis spectrophotometer and cooled down to 238 K. After reaching thermal equilibrium an UV/Vis ab-

sorption spectrum of the starting complex was recorded. Then, 50 μL of a solution containing tetrabutylammonium periodate in dry acetonitrile were added (3 μmols). The formation of a band at $\lambda_{max}=780$ nm ($\varepsilon=80\ M^{-1}\ cm^{-1}$) with a weak shoulder at 930 nm was observed.

Computational details. Density functional theory (DFT) calculations were performed with the Gaussian09 rev. D.01 software package.[72] The X-ray diffracted structure of complex $[Fe^{II}(OTf)_2(PyNMe_3)]$ (**1**)[38] has been chosen as starting point for geometry optimizations, using the hybrid B3LYP exchange-correlation functional[73–75] in conjunction with the 6-31G(d,p) 6d basis set on all atoms. The two electron-integrals were evaluated numerically with a high accurate grid using the integral = ultrafine keyword. The effect of the acetonitrile solvent in geometry optimization calculations was modelled through the SMD continuum solvation model.[76] Van der Waals interactions were included using the Grimme-D3 correction with the Becke-Johnson damping.[77] The molecular structures have been edited with the Chemcraft program.[78]

The nature of the stationary points was characterized by vibrational analyses in the same level of theory as geometry optimizations, where minima have no imaginary frequencies and transition states only one. Frequency calculations on the stationary points were also employed to evaluate the thermal contribution to the Gibbs energies (G_{corr}) at 233.15 K.

The final free energies (G) were further refined by single point calculations with the cc-pVTZ 6d dunning basis set on the equilibrium geometries, including the solvent and dispersion effects ($E_{cc-pvtz}$):

$$G = E_{cc-pvtz} + G_{corr} \quad (1)$$

The employed triflic acid in experiments should be completely dissociated due to the low pKa value (2.6) that presents in acetonitrile. Therefore, in the protonation reactions the free energy of the proton in acetonitrile $G\left(H^+_{sol}\right)$ has been considered:

$$G\left(H^+_{sol}\right) = G\left(H^+_{gas}\right) + \Delta G^{H+}_{solv} \quad (2)$$

In which (ΔG^{H+}_{solv}) is the proton solvation free energy in acetonitrile ($\Delta G^{H+}_{solv} = -260.2\ kcal \cdot mol^{-1}$)[79] and its gas-phase free energy at 233.15 K ($G\left(H^+_{gas}\right) = -4.6\ kcal \cdot mol^{-1}$).

In the energy balances, the free-energy change of moving from a 1 atm of pressure to the desired concentration ($\Delta G^{o/*}$) was also considered.[79] $\Delta G^{o/*}$ values are derived with the following equation:

$$\Delta G^{o/*} = RT\ \ln(24.4 \times c) \quad (3)$$

In which R is the universal gas constant ($1.987\ cal\,mol^{-1}\cdot K^{-1}$), T is the temperature in Kelvin and c the concentration in $mol\,L^{-1}$. The $\Delta G^{\circ}/*$ correction at 233.15 K is $1.5\ kcal\,mol^{-1}$ and $-1.7\ kcal\,mol^{-1}$ for 1.0 M standard state substrates and 1.1 mM of protons (1.1 mM of triflic acid), respectively. Concentrations of 19.1 M and 5.0 mM were employed for the explicit solvent acetonitrile and water molecules (derived from the hydrogen peroxide solution), respectively, which translate into $\Delta G^{\circ}/*$ values of $2.8\ kcal\,mol^{-1}$ and $-1.0\ kcal\,mol^{-1}$.

Labels **R**, **TS** and **P** were used as short nomenclature of reactant complexes, transition states and products involved in the O–O bond cleavage mechanisms. The subscripts **d** and **q** are used to specify the doublet and quartet spin states of the iron intermediates, respectively.

Acknowledgements

Financial support for this work was provided by the European Commission (2011-CIG-303522 to A.C., 675020-MSCA-ITN-2015-ETN to M.C.), the Spanish Ministry of Science (CTQ2015-70795-P to M.C., CTQ2016-77989-P to A.C., CTQ2014-52525-P to J.M.L., CTQ2015-65707-C2-2-P to M.G.B., and CSD2010-00065 to M.C and M.G.B.) and Generalitat de Catalunya (ICREA Academia Award to M.C. and 2014 SGR 862). The Spanish Ministry of Science is also acknowledged for a Ramón *y* Cajal contract to A.C. (RYC-2011–08683). The work conducted at the University of Minnesota has been supported by the US National Science Foundation (grant CHE1665391 to L.Q.). XAS data was collected at the SOLEIL synchrotron SAMBA beamline (proposal 20150413). We would like to thank the beamline staff for their help with experiment preparation in particular Dr. Andrea Zitolo.

Conflict of interest

The authors declare no conflict of interest.

Keywords: C–H bond activation · density functional calculations · hydroperoxoiron(III) · stereospecific · oxidation

[1] R. M. Burger, T. A. Kent, S. B. Horwitz, E. Münck, J. Peisach, *J. Biol. Chem.* **1983**, *258*, 1559 – 1564.
[2] M. S. Chow, L. V. Liu, E. I. Solomon, *Proc. Natl. Acad. Sci. USA* **2008**, *105*, 13241 – 13245.
[3] S. M. Hecht, *Acc. Chem. Res.* **1986**, *19*, 383 – 391.
[4] S. M. Barry, G. L. Challis, *ACS Catal.* **2013**, *3*, 2362 – 2370.
[5] D. J. Ferraro, E. N. Brown, C.-L. Yu, R. E. Parales, D. T. Gibson, S. Ramaswamy, *BMC Struct. Biol.* **2007**, *7*, 10.
[6] D. J. Ferraro, L. Gakhar, S. Ramaswamy, *Biochem. Biophys. Res. Commun.* **2005**, *338*, 175 – 190.
[7] Y. Ashikawa, Z. Fujimoto, Y. Usami, K. Inoue, H. Noguchi, H. Yamane, H. Nojiri, *BMC Struct. Biol.* **2012**, *12*, 15.
[8] A. Karlsson, J. V. Parales, R. E. Parales, D. T. Gibson, H. Eklund, S. Ramaswamy, *Science* **2003**, *299*, 1039 – 1042.
[9] A. Decker, M. S. Chow, J. N. Kemsley, N. Lehnert, E. I. Solomon, *J. Am. Chem. Soc.* **2006**, *128*, 4719 – 4733.
[10] F. Neese, J. M. Zaleski, K. Loeb Zaleski, E. I. Solomon, *J. Am. Chem. Soc.* **2000**, *122*, 11703 – 11724.
[11] D. Kumar, H. Hirao, S. Shaik, P. M. Kozlowski, *J. Am. Chem. Soc.* **2006**, *128*, 16148 – 16158.
[12] A. Thibon, V. Jollet, C. Ribal, K. Sénéchal-David, L. Billon, A. B. Sorokin, F. Banse, *Chem. Eur. J.* **2012**, *18*, 2715 – 2724.
[13] A. Company, J. Lloret-Fillol, M. Costas, in *Comprehensive Inorganic Chemistry II, (Second Edition)*, Elsevier, Amsterdam, **2013**, pp. 487 – 564.
[14] M. Costas, M. P. Mehn, M. P. Jensen, L. Que, *Chem. Rev.* **2004**, *104*, 939 – 986.
[15] S. Hong, Y.-M. Lee, W. Shin, S. Fukuzumi, W. Nam, *J. Am. Chem. Soc.* **2009**, *131*, 13910 – 13911.
[16] A. Thibon, J. England, M. Martinho, V. G. Young, J. R. Frisch, R. Guillot, J.-J. Girerd, E. Münck, L. Que, F. Banse, *Angew. Chem. Int. Ed.* **2008**, *47*, 7064 – 7067; *Angew. Chem.* **2008**, *120*, 7172 – 7175.
[17] I. G. Denisov, T. M. Makris, S. G. Sligar, I. Schlichting, *Chem. Rev.* **2005**, *105*, 2253 – 2278.
[18] A. R. Groenhof, A. W. Ehlers, K. Lammertsma, *J. Am. Chem. Soc.* **2007**, *129*, 6204 – 6209.
[19] S. G. Sligar, T. M. Makris, I. G. Denisov, *Biochem. Biophys. Res. Commun.* **2005**, *338*, 346 – 354.

[20] W. Nam, H. J. Han, S.-Y. Oh, Y. J. Lee, M.-H. Choi, S.-Y. Han, C. Kim, S. K. Woo, W. Shin, *J. Am. Chem. Soc.* **2000**, *122*, 8677 – 8684.
[21] S. J. Yang, W. Nam, *Inorg. Chem.* **1998**, *37*, 606 – 607.
[22] K. Chen, M. Costas, J. Kim, A. K. Tipton, L. Que, *J. Am. Chem. Soc.* **2002**, *124*, 3026 – 3035.
[23] O. V. Makhlynets, E. V. Rybak-Akimova, *Chem. Eur. J.* **2010**, *16*, 13995 – 14006.
[24] R. Mas-Ballesté, L. Que, *J. Am. Chem. Soc.* **2007**, *129*, 15964 – 15972.
[25] I. Prat, A. Company, V. Postils, X. Ribas, L. Q. Jr., J. M. Luis, M. Costas, *Chem. Eur. J.* **2013**, *19*, 6724 – 6738.
[26] F. Wang, W. Sun, C. Xia, Y. Wang, *J. Biol. Inorg. Chem.* **2017**, *22*, 987 – 998.
[27] A. Ansari, A. kaushik, G. Rajaraman, *J. Am. Chem. Soc.* **2013**, *135*, 4235 – 4249.
[28] A. Bassan, M. R. A. Blomberg, P. E. M. Siegbahn, L. Que, *J. Am. Chem. Soc.* **2002**, *124*, 11056 – 11063.
[29] A. Bassan, M. R. A. Blomberg, P. E. M. Siegbahn, *J. Biol. Inorg. Chem.* **2004**, *9*, 439 – 452.
[30] W. N. Oloo, A. J. Fielding, L. Que, *J. Am. Chem. Soc.* **2013**, *135*, 6438 – 6441.
[31] S. Bang, S. Park, Y.-M. Lee, S. Hong, K.-B. Cho, W. Nam, *Angew. Chem. Int. Ed.* **2014**, *53*, 7843 – 7847; *Angew. Chem.* **2014**, *126*, 7977 – 7981.
[32] S. Chatterjee, T. K. Paine, *Angew. Chem. Int. Ed.* **2015**, *54*, 9338 – 9342; *Angew. Chem.* **2015**, *127*, 9470 – 9474.
[33] S. Chatterjee, T. K. Paine, *Angew. Chem. Int. Ed.* **2016**, *55*, 7717 – 7722.
[34] L. V. Liu, S. Hong, J. Cho, W. Nam, E. I. Solomon, *J. Am. Chem. Soc.* **2013**, *135*, 3286 – 3299.
[35] N. Lehnert, R. Y. N. Ho, L. Que, E. I. Solomon, *J. Am. Chem. Soc.* **2001**, *123*, 12802 – 12816.
[36] F. Li, K. K. Meier, M. A. Cranswick, M. Chakrabarti, K. M. Van Heuvelen, E. Münck, L. Que, *J. Am. Chem. Soc.* **2011**, *133*, 7256 – 7259.
[37] C. Miao, B. Wang, Y. Wang, C. Xia, Y.-M. Lee, W. Nam, W. Sun, *J. Am. Chem. Soc.* **2016**, *138*, 936 – 943.
[38] J. Serrano-Plana, W. N. Oloo, L. Acosta-Rueda, K. K. Meier, B. Verdejo, E. García-España, M. G. Basallote, E. Münck, L. Que, A. Company, M. Costas, *J. Am. Chem. Soc.* **2015**, *137*, 15833 – 15842.
[39] J. Serrano-Plana, A. Aguinaco, R. Belda, E. García-España, M. G. Basallote, A. Company, M. Costas, *Angew. Chem. Int. Ed.* **2016**, *55*, 6310 – 6314; *Angew. Chem.* **2016**, *128*, 6418 – 6422.
[40] C. Kim, K. Chen, J. Kim, L. Que, *J. Am. Chem. Soc.* **1997**, *119*, 5964 – 5965.
[41] G. Roelfes, M. Lubben, K. Chen, R. Y. N. Ho, A. Meetsma, S. Genseberger, R. M. Hermant, R. Hage, S. K. Mandal, V. G. Young, Y. Zang, H. Kooijman, A. L. Spek, L. Que, B. L. Feringa, *Inorg. Chem.* **1999**, *38*, 1929 – 1936.
[42] R. Y. N. Ho, G. Roelfes, B. L. Feringa, L. Que, *J. Am. Chem. Soc.* **1999**, *121*, 264 – 265.
[43] G. Roelfes, V. Vrajmasu, K. Chen, R. Y. N. Ho, J.-U. Rohde, C. Zondervan, R. M. la Crois, E. P. Schudde, M. Lutz, A. L. Spek, R. Hage, B. L. Feringa, E. Münck, L. Que, *Inorg. Chem.* **2003**, *42*, 2639 – 2653.
[44] C. P. S. Taylor, *BBA-Protein Struct.* **1977**, *491*, 137 – 148.
[45] B. R. McGarvey, *Coord. Chem. Rev.* **1998**, *170*, 75 – 92.
[46] K. D. Koehntop, J.-U. Rohde, M. Costas, L. Que Jr, *Dalton Trans.* **2004**, 3191 – 3198.
[47] X. Shan, J.-U. Rohde, K. D. Koehntop, Y. Zhou, M. R. Bukowski, M. Costas, K. Fujisawa, L. Que, *Inorg. Chem.* **2007**, *46*, 8410 – 8417.
[48] J. Stasser, F. Namuswe, G. D. Kasper, Y. Jiang, C. M. Krest, M. T. Green, J. Penner-Hahn, D. P. Goldberg, *Inorg. Chem.* **2010**, *49*, 9178 – 9190.
[49] J. Shearer, R. C. Scarrow, J. A. Kovacs, *J. Am. Chem. Soc.* **2002**, *124*, 11709 – 11717.
[50] Y. He, C. R. Goldsmith, *Chem. Commun.* **2012**, *48*, 10532 – 10534.
[51] Y. Mekmouche, H. Hummel, R. Y. N. Ho, J. L. Que, V. Schünemann, F. Thomas, A. X. Trautwein, C. Lebrun, K. Gorgy, J.-C. Leprêtre, M.-N. Collomb, A. Deronzier, M. Fontecave, S. Ménage, *Chem. Eur. J.* **2002**, *8*, 1196 – 1204.
[52] E. A. Mikhalyova, O. V. Makhlynets, T. D. Palluccio, A. S. Filatov, E. V. Rybak-Akimova, *Chem. Commun.* **2012**, *48*, 687 – 689.
[53] J. Cho, S. Jeon, S. A. Wilson, L. V. Liu, E. A. Kang, J. J. Braymer, M. H. Lim, B. Hedman, K. O. Hodgson, J. S. Valentine, E. I. Solomon, W. Nam, *Nature* **2011**, *478*, 502 – 505.
[54] M. Puri, L. Que, *Acc. Chem. Res.* **2015**, *48*, 2443 – 2452.
[55] M. J. Park, J. Lee, Y. Suh, J. Kim, W. Nam, *J. Am. Chem. Soc.* **2006**, *128*, 2630 – 2634.
[56] Significant amounts of byproducts resulting from secondary C–H oxidation were also detected in the oxidation of *cis*-1,2-dimethylcyclohexane by **3** in the absence of acid.
[57] J. Park, Y. Morimoto, Y.-M. Lee, W. Nam, S. Fukuzumi, *J. Am. Chem. Soc.* **2012**, *134*, 3903 – 3911.
[58] I. M. Kolthoff, M. K. Chantooni, *J. Am. Chem. Soc.* **1973**, *95*, 8539 – 8546.
[59] T. Fujinaga, I. Sakamoto, *J. Electroanal. Chem. Interfacial Electrochem.* **1977**, *85*, 185 – 201.
[60] R. H. Morris, *Chem. Rev.* **2016**, *116*, 8588 – 8654.
[61] H. Hirao, F. Li, L. Que, K. Morokuma, *Inorg. Chem.* **2011**, *50*, 6637 – 6648.
[62] J. Bautz, M. R. Bukowski, M. Kerscher, A. Stubna, P. Comba, A. Lienke, E. Münck, L. Que, *Angew. Chem. Int. Ed.* **2006**, *45*, 5681 – 5684; *Angew. Chem.* **2006**, *118*, 5810 – 5813.
[63] J. Kaizer, M. Costas, L. Que, *Angew. Chem. Int. Ed.* **2003**, *42*, 3671 – 3673; *Angew. Chem.* **2003**, *115*, 3799 – 3801.
[64] ASTM E1840-1896 (2007) Standard Guide for Raman Shift Standards for Spectrometer Calibration, ASTM International, DOI: 1810.1520/E1840-1896R1807.
[65] M. Newville, *J. Synchrotron Radiat.* **2001**, *8*, 96 – 100.
[66] B. Ravel, M. Newville, *J. Synchrotron Radiat.* **2005**, *12*, 537 – 541.
[67] J. J. Rehr, R. C. Albers, *Rev. Mod. Phys.* **2000**, *72*, 621 – 654.
[68] K. Banaszak, V. Martin-Diaconescu, M. Bellucci, B. Zambelli, W. Rypniewski, M. J. Maroney, S. Ciurli, *Biochem. J.* **2012**, *441*, 1017 – 1026.
[69] V. Martin-Diaconescu, M. Bellucci, F. Musiani, S. Ciurli, M. J. Maroney, *J. Biol. Inorg. Chem.* **2012**, *17*, 353 – 361.
[70] B. Zambelli, A. Berardi, V. Martin-Diaconescu, L. Mazzei, F. Musiani, M. J. Maroney, S. Ciurli, *J. Biol. Inorg. Chem.* **2014**, *19*, 319 – 334.
[71] R. W. Herbst, I. Perovic, V. Martin-Diaconescu, K. O'Brien, P. T. Chivers, S. S. Pochapsky, T. C. Pochapsky, M. J. Maroney, *J. Am. Chem. Soc.* **2010**, *132*, 10338 – 10351.
[72] F. Gaussian 09 Revision D.01, M. J.; Trucks, G. W.; Schlegel, H. B.; Scuseria, G. E.; Robb, M. A.; Cheeseman, J. R.; Scalmani, G.; Barone, V.; Mennucci, B.; Petersson, G. A.; Nakatsuji, H.; Caricato, M.; Li, X.; Hratchian, H. P.; Izmaylov, A. F.; Bloino, J.; Zheng, G.; Sonnenberg, J. L.; Hada, M.; Ehara, M.; Toyota, K.; Fukuda, R.; Hasegawa, J.; Ishida, M.; Nakajima, T.; Honda, Y.; Kitao, O.; Nakai, H.; Vreven, T.; Montgomery, Jr., J. A.; Peralta, J. E.; Ogliaro, F.; Bearpark, M.; Heyd, J. J.; Brothers, E.; Kudin, K. N.; Staroverov, V. N.; Kobayashi, R.; Normand, J.; Raghavachari, K.; Rendell, A.; Burant, J. C.; Iyengar, S. S.; Tomasi, J.; Cossi, M.; Rega, N.; Millam, J. M.; Klene, M.; Knox, J. E.; Cross, J. B.; Bakken, V.; Adamo, C.; Jaramillo, J.; Gomperts, R.; Stratmann, R. E.; Yazyev, O.; Austin, A. J.; Cammi, R.; Pomelli, C.; Ochterski, J. W.; Martin, R. L.; Morokuma, K.; Zakrzewski, V. G.; Voth, G. A.; Salvador, P.; Dannenberg, J. J.; Dapprich, S.; Daniels, A. D.; Farkas, Ö.; Foresman, J. B.; Ortiz, J. V.; Cioslowski, J.; Fox, D. J., Gaussian, Inc., Wallingford CT, **2009**.
[73] A. D. Becke, *J. Chem. Phys.* **1993**, *98*, 5648.
[74] A. D. Becke, *J. Chem. Phys.* **1993**, *98*, 1372.
[75] C. Lee, W. Yang, R. G. Parr, *Phys. Chem. Rev. B* **1988**, *37*, 785.
[76] A. V. Marenich, C. J. Cramer, D. G. Truhlar, *J. Phys. Chem. B* **2009**, *113*, 6378 – 6396.
[77] S. Grimme, S. Ehrlich, L. Goerigk, *J. Comput. Chem.* **2011**, *32*, 1456 – 1465.
[78] http://www.chemcraftprog.com.
[79] C. P. Kelly, C. J. Cramer, D. G. Truhlar, *J. Phys. Chem. A* **2006**, *110*, 2493 – 2499.

Manuscript received: October 13, 2017
Accepted manuscript online: November 28, 2017
Version of record online: January 16, 2018